A high order hybrid mimetic discretization on curvilinear quadrilateral meshes for complex geometries

Zhang, Yi; Jain, Varun; Palha da Silva Clérigo, Artur; Gerritsma, Marc

Publication date
2020

Document Version
Accepted author manuscript

Published in
Proceedings of the 6th European Conference on Computational Mechanics

6th European Conference on Computational Mechanics (ECCM 6)
7th European Conference on Computational Fluid Dynamics (ECFD 7)
11-15 June 2018, Glasgow, UK

A HIGH ORDER HYBRID MIMETIC DISCRETIZATION ON CURVILINEAR QUADRILATERAL MESHES FOR COMPLEX GEOMETRIES

Yi Zhang[1], Varun Jain[1], Artur Palha[2] and Marc Gerritsma[1]

[1] Delft University of Technology
Kluyverweg 1, 2629 HS Delft, Netherlands
{y.zhang-14, v.jain, m.i.gerritsma}@tudelft.nl

[2] Eindhoven University of Technology
5612 AZ Eindhoven, Netherlands
a.palha@tue.nl

Key words: Hybridization, Mimetic Spectral Element Method, Broken Spaces, Algebraic Dual Polynomials, Mixed Poisson Formulation.

Abstract. In this paper, we present a hybrid mimetic method which solves the mixed formulation of the Poisson problem on curvilinear quadrilateral meshes. The method is hybrid in the sense that the domain is decomposed into multiple disjoint elements and the interelement continuity is enforced using a Lagrange multiplier. The method is mimetic in the sense that the discrete divergence operator is exact. By using the mimetic basis functions and their dual representations, various metric-free discrete terms are obtained. The discrete system can be efficiently solved by first solving a reduced system for the Lagrange multiplier. Numerical experiments which validate the method are presented.

1 INTRODUCTION

Hybrid methods weaken the continuity across the interelement boundary by introducing a Lagrange multiplier between elements. It looks like hybrid methods complicate the problem, but they decompose the domain which benefits the computation significantly. For example, hybrid methods result in easily parallelizable systems. Hybrid methods were first introduced in computational solid mechanics. The pioneering work was released in [11] where a finite element method based on a new variational principle assuming compatible displacement functions along the interelement boundary in addition to the equilibrium stress field in each element was presented. Another classic example is the primal hybrid finite element method presented in [12].

Mimetic methods aim to preserve the structure of partial differential equations at the discrete level. Therefore, mimetic methods are also called structure-preserving or compatible methods. A key feature of mimetic finite element methods is that their function spaces satisfy the De Rham complex, [1]. The mimetic spectral element method, [5, 8, 9, 10], is a

high order mimetic finite element method. This method uses the mathematical language of differential geometry and constructs the so-called mimetic basis functions (polynomials) which also work for curvilinear quadrilateral meshes. We will use these basis functions and their algebraic dual representations, [7], but in the conventional mathematical language of vector calculus.

In this paper, we combine these two ideas and construct a high order method which is then used to solve a hybrid mixed formulation of the Poisson equation. The method is hybrid; elements are discontinuous and interelement continuity is enforced with a Lagrange multiplier. It is mimetic; the divergence operator is preserved at the discrete level. In addition, only one block of the discrete system will be metric-dependent. The remaining blocks are metric-free, extremely sparse and finite-difference(volume)-like (containing non-zero entries of -1 and 1 only). These features make the method a preferable one especially for complex computational domains.

This paper is organized as follows: In Section 2, we introduce the necessary definitions and notations. In Section 3, a hybrid mixed formulation of the Poisson equation is derived. In Section 4, mimetic basis functions and their dual representations are presented. The discretization with these basis functions follows in Section 5. Finally, two numerical experiments are presented in Section 6.

2 PRELIMINARIES AND NOTATIONS

Given an open bounded domain $\Omega \subset \mathbb{R}^d$ with Lipschitz boundary $\partial\Omega$, let $L^2(\Omega)$ denote the space of square integrable scalar-valued functions defined in Ω and

$$H^1(\Omega) := \left\{ \varphi \in L^2(\Omega) \,\middle|\, \text{grad}\, \varphi \in \left[L^2(\Omega)\right]^d \right\},$$

$$H(\text{div}, \Omega) := \left\{ \boldsymbol{u} \in \left[L^2(\Omega)\right]^d \,\middle|\, \text{div}\, \boldsymbol{u} \in L^2(\Omega) \right\}.$$

Trace operators tr_{grad} and tr_{div} restrict $\varphi \in H^1(\Omega)$ and $\boldsymbol{u} \in H(\text{div}, \Omega)$ onto $\partial\Omega$ respectively:

$$\text{tr}_{\text{grad}}\varphi = \varphi|_{\partial\Omega}\,, \;\; \text{tr}_{\text{div}}\boldsymbol{u} = \boldsymbol{u}|_{\partial\Omega} \cdot \boldsymbol{n}_\Omega,$$

where $\boldsymbol{n}_\Omega$ represents the unit outward normal of $\partial\Omega$. Spaces $H^{1/2}(\partial\Omega)$ and $H^{-1/2}(\partial\Omega)$ are then defined as

$$H^{1/2}(\partial\Omega) := \text{tr}_{\text{grad}} H^1(\Omega),$$
$$H^{-1/2}(\partial\Omega) := \text{tr}_{\text{div}} H(\text{div}, \Omega).$$

With a mesh, denoted by Ω_h, which partitions Ω into K disjoint open elements Ω_k with Lipschitz boundary $\partial\Omega_k$,

$$\bar{\Omega} = \bigcup_{k=1}^{K} \bar{\Omega}_k, \;\; \Omega_i \cap \Omega_j = \emptyset, \;\; 1 \leq i \neq j \leq K,$$

we can break $H^1(\Omega), H(\text{div}, \Omega)$ and obtain the so-called broken Sobolev spaces,

$$H^1(\Omega_h) = \left\{ \varphi \in L^2(\Omega) \middle|\, \varphi|_{\Omega_k} \in H^1(\Omega_k) \right\} = \prod_{k=1}^{K} H^1(\Omega_k),$$

$$H(\mathrm{div},\Omega_h)=\left\{\boldsymbol{u}\in\left[L^2(\Omega)\right]^d\middle|\ \boldsymbol{u}|_{\Omega_k}\in H(\mathrm{div},\Omega_k)\right\}=\prod_{k=1}^{K}H(\mathrm{div},\Omega_k).$$

Spaces for interface functions are then defined as

$$H^{1/2}(\partial\Omega_h):=\mathrm{tr}^h_{\mathrm{grad}}H^1(\Omega),$$

$$H^{-1/2}(\partial\Omega_h):=\mathrm{tr}^h_{\mathrm{div}}H(\mathrm{div},\Omega),$$

where trace operators $\mathrm{tr}^h_{\mathrm{grad}}$ and $\mathrm{tr}^h_{\mathrm{div}}$ restrict $\varphi\in H^1(\Omega)$ and $\boldsymbol{u}\in H(\mathrm{div},\Omega)$ respectively onto $\partial\Omega_h=\bigcup_{k=1}^{K}\partial\Omega_k$. For broken spaces, trace operators $\mathrm{tr}_{\mathrm{grad}}$ and $\mathrm{tr}_{\mathrm{div}}$ are linear mappings:

$$\mathrm{tr}_{\mathrm{grad}}:H^1(\Omega_h)\to\prod_{k=1}^{K}H^{1/2}(\partial\Omega_k),$$

$$\mathrm{tr}_{\mathrm{div}}:H(\mathrm{div},\Omega_h)\to\prod_{k=1}^{K}H^{-1/2}(\partial\Omega_k).$$

Clearly, in general $\mathrm{tr}_{\mathrm{grad}}\neq\mathrm{tr}^h_{\mathrm{grad}}$ and $\mathrm{tr}_{\mathrm{div}}\neq\mathrm{tr}^h_{\mathrm{div}}$.

For more information about Sobolev spaces, see [13]. A comprehensive introduction about broken Sobolev spaces is given in [2].

3 THE HYBRID WEAK FORMULATION

We consider the constrained minimization problem,

$$\underset{\boldsymbol{u}\in L^2(\Omega)}{\arg}\ \min_{\mathrm{div}\boldsymbol{u}=-f}\frac{1}{2}\left(\boldsymbol{u},\boldsymbol{u}\right)_{L^2(\Omega)},$$

where $f\in L^2(\Omega)$ is given. Notice that this problem is not well-posed yet because no boundary condition is prescribed. By introducing a Lagrange multiplier φ, we can rewrite this constrained minimization problem into a saddle-point problem for $(\boldsymbol{u},\varphi)\in H(\mathrm{div},\Omega)\times H^1(\Omega)$:

$$\mathcal{L}(\boldsymbol{u},\varphi;f,\hat{\varphi})=\frac{1}{2}\left(\boldsymbol{u},\boldsymbol{u}\right)_{L^2(\Omega)}+\left(\varphi,\mathrm{div}\ \boldsymbol{u}+f\right)_{L^2(\Omega)}-\left(\hat{\varphi},\mathrm{tr}_{\mathrm{div}}\boldsymbol{u}\right)_{L^2(\partial\Omega)},\tag{1}$$

where $\hat{\varphi}=\mathrm{tr}_{\mathrm{grad}}\ \varphi\in H^{1/2}(\partial\Omega)$ is given. Variational analysis on this functional gives rise to the mixed formulation: *Find* $(\boldsymbol{u},\varphi)\in H(\mathrm{div},\Omega)\times H^1(\Omega)$ *such that*

$$\begin{cases}\left(\boldsymbol{u},\boldsymbol{v}\right)_{L^2(\Omega)}+\left(\varphi,\mathrm{div}\ \boldsymbol{v}\right)_{L^2(\Omega)} &=\left(\hat{\varphi},\mathrm{tr}_{\mathrm{div}}\boldsymbol{v}\right)_{L^2(\partial\Omega)}\\ \left(\psi,\mathrm{div}\ \boldsymbol{u}\right)_{L^2(\Omega)} &=-\left(\psi,f\right)_{L^2(\Omega)}\end{cases},\tag{2}$$

for all $(\boldsymbol{v},\psi)\in H(\mathrm{div},\Omega)\times H^1(\Omega)$. This is a weak formulation of the Poisson equation.

If we set up a mesh Ω_h in Ω, by breaking $\boldsymbol{u}$ and φ into broken spaces, $H(\mathrm{div}, \Omega_h)$ and $H^1(\Omega_h)$, and introducing a new Lagrange multiplier $\check{\varphi}$ in the interface space $H^{1/2}(\partial\Omega_h \backslash \partial\Omega)$, we can rewrite (1) as

$$\mathcal{L}(\boldsymbol{u}, \varphi, \check{\varphi}; f, \hat{\varphi}) = \frac{1}{2}(\boldsymbol{u}, \boldsymbol{u})_{L^2(\Omega)} + (\varphi, \mathrm{div}\ \boldsymbol{u} + f)_{L^2(\Omega)} - (\check{\varphi}, \mathrm{tr}_{\mathrm{div}}\boldsymbol{u})_{L^2(\partial\Omega_h \backslash \partial\Omega)} - (\hat{\varphi}, \mathrm{tr}_{\mathrm{div}}\boldsymbol{u})_{L^2(\partial\Omega)}. \quad (3)$$

Consider the interface Γ_{ij} shared by two elements, Ω_i and Ω_j,

$$\Gamma_{ij} = \partial\Omega_i \cap \partial\Omega_j \neq \emptyset,\ 1 \leq i \neq j \leq K.$$

To retrieve the interelement continuity of broken $\boldsymbol{u}$, relation

$$(\mathrm{tr}_{\mathrm{div}}\boldsymbol{u})|_{\Gamma_{ij}} = \boldsymbol{u}|_{\partial\Omega_i} \cdot \boldsymbol{n}_{\partial\Omega_i} + \boldsymbol{u}|_{\partial\Omega_j} \cdot \boldsymbol{n}_{\partial\Omega_j} = 0, \quad (4)$$

needs to hold. The interface variable $\check{\varphi}$ in functional (3) serves as the Lagrange multiplier which enforces (4) at the interface $\partial\Omega_h \backslash \partial\Omega$. From functional (3), we can obtain the hybrid mixed formulation for the Poisson problem written as: *Given* $f \in L^2(\Omega)$ *and* $\hat{\varphi} = \mathrm{tr}_{\mathrm{grad}}\ \varphi \in H^{1/2}(\partial\Omega)$*, find* $(\boldsymbol{u}, \varphi, \check{\varphi}) \in H(\mathrm{div}, \Omega_h) \times H^1(\Omega_h) \times H^{1/2}(\partial\Omega_h \backslash \partial\Omega)$ *such that*

$$\begin{cases} (\boldsymbol{u}, \boldsymbol{v})_{L^2(\Omega)} + (\varphi, \mathrm{div}\ \boldsymbol{v})_{L^2(\Omega)} - (\check{\varphi}, \mathrm{tr}_{\mathrm{div}}\boldsymbol{v})_{L^2(\partial\Omega_h \backslash \partial\Omega)} & = (\hat{\varphi}, \mathrm{tr}_{\mathrm{div}}\boldsymbol{v})_{L^2(\partial\Omega)} \\ (\psi, \mathrm{div}\ \boldsymbol{u})_{L^2(\Omega)} & = -(\psi, f)_{L^2(\Omega)} \\ -(\check{\psi}, \mathrm{tr}_{\mathrm{div}}\boldsymbol{u})_{L^2(\partial\Omega_h \backslash \partial\Omega)} & = 0 \end{cases},$$

for all $(\boldsymbol{v}, \psi, \check{\psi}) \in H(\mathrm{div}, \Omega_h) \times H^1(\Omega_h) \times H^{1/2}(\partial\Omega_h \backslash \partial\Omega)$. It is easy to prove that the interface variable $\check{\varphi}$ represents the restriction of φ onto $\partial\Omega_h \backslash \partial\Omega$.

4 BASIS FUNCTIONS

In this section, we briefly introduce the mimetic basis functions, [8, 9, 10], and their algebraic dual representations, [7].

4.1 Mimetic basis functions

Let $-1 = \xi_0 < \xi_1 < \cdots < \xi_N = 1$ be a partitioning of the interval $[-1, 1]$. The associated Lagrange polynomials are

$$h_i(\xi),\ \xi \in [-1, 1],\ i = 0, 1, \cdots, N,$$

which satisfy $h_i(\xi_j) = \delta_{i,j}$, where $\delta_{i,j}$ is the Kronecker delta. The corresponding edge functions are then defined as, [4],

$$e_i(\xi) = -\sum_{k=0}^{i-1} \frac{\mathrm{d}h_k(\xi)}{\mathrm{d}\xi} = \sum_{k=i}^{N} \frac{\mathrm{d}h_k(\xi)}{\mathrm{d}\xi},\ i = 1, 2, \cdots, N,$$

which satisfy $\int_{\xi_{j-1}}^{\xi_j} e_i(\xi) = \delta_{i,j}$.

From now on, we restrict ourselves to $\mathbb{R}^2$. The extension to higher dimensions is straightforward. Consider the reference domain $\Omega_{\text{ref}}|\,(\xi,\eta) = [-1,1]^2$ in $\mathbb{R}^2$. By applying above partitioning along two axes (which does not have to be the case; partitionings along two axes can be different), we obtain basis functions $\{h_i(\xi)e_j(\eta), e_i(\xi)h_j(\eta)\}$ and $\{e_i(\xi)e_j(\eta)\}$.

A vector field $\boldsymbol{u} = (u,v)^T$ can be expanded in term of $\{h_i(\xi)e_j(\eta), e_i(\xi)h_j(\eta)\}$ into

$$\boldsymbol{u}_h = \left(\sum_{i=0}^{N}\sum_{j=1}^{N} u_{i,j} h_i(\xi)e_j(\eta), \sum_{i=1}^{N}\sum_{j=0}^{N} v_{i,j} e_i(\xi)h_j(\eta) \right)^T, \tag{5}$$

where

$$u_{i,j} = \int_{\eta_{j-1}}^{\eta_j} u(\xi_i,\eta)\mathrm{d}\eta,\ \ v_{i,j} = \int_{\xi_{i-1}}^{\xi_i} v(\xi,\eta_j)\mathrm{d}\xi.$$

A scalar function f can be expanded in terms of $\{e_i(\xi)e_j(\eta)\}$ into

$$f_h = \sum_{i=1}^{N}\sum_{j=1}^{N} f_{i,j} e_i(\xi)e_j(\eta), \tag{6}$$

where

$$f_{i,j} = \int_{\xi_{i-1}}^{\xi_i}\int_{\eta_{j-1}}^{\eta_j} f(\xi,\eta)\mathrm{d}\xi\mathrm{d}\eta.$$

If relation $f = \text{div}\ \boldsymbol{u}$ holds, the discrete relation,

$$f_h = \text{div}\ \boldsymbol{u}_h = \sum_{i=1}^{N}\sum_{j=1}^{N} \left(u_{i,j} - u_{i-1,j} + v_{i,j} - v_{i,j-1}\right) e_i(\xi)e_j(\eta), \tag{7}$$

will also hold. Let $\underline{\boldsymbol{u}}$ and $\underline{f}$ be column vectors of the expansion coefficients of $\boldsymbol{u}_h$ and f_h. Throughout the rest of this paper, underlined variables will always represent the column vectors of the expansion coefficients of the discrete variables. From (7), we can derive

$$\underline{f} = \mathbb{E}^{2,1}\underline{\boldsymbol{u}},$$

where $\mathbb{E}^{2,1}$ is the incidence matrix which only depends on the labeling of the expansion coefficients and only contains non-zero entries of -1 and 1. For example, the incidence matrix for the reference domain in Figure 1 is given by

$$\mathbb{E}^{2,1} = \begin{pmatrix}
-1 & 1 & 0 & 0 & 0 & 0 & 0 & 0 & 0 & 0 & 0 & 0 & -1 & 0 & 0 & 1 & 0 & 0 & 0 & 0 & 0 & 0 & 0 & 0 \\
0 & -1 & 1 & 0 & 0 & 0 & 0 & 0 & 0 & 0 & 0 & 0 & 0 & -1 & 0 & 0 & 1 & 0 & 0 & 0 & 0 & 0 & 0 & 0 \\
0 & 0 & -1 & 1 & 0 & 0 & 0 & 0 & 0 & 0 & 0 & 0 & 0 & 0 & -1 & 0 & 0 & 1 & 0 & 0 & 0 & 0 & 0 & 0 \\
0 & 0 & 0 & 0 & -1 & 1 & 0 & 0 & 0 & 0 & 0 & 0 & 0 & 0 & 0 & -1 & 0 & 0 & 1 & 0 & 0 & 0 & 0 & 0 \\
0 & 0 & 0 & 0 & 0 & -1 & 1 & 0 & 0 & 0 & 0 & 0 & 0 & 0 & 0 & 0 & -1 & 0 & 0 & 1 & 0 & 0 & 0 & 0 \\
0 & 0 & 0 & 0 & 0 & 0 & -1 & 1 & 0 & 0 & 0 & 0 & 0 & 0 & 0 & 0 & 0 & -1 & 0 & 0 & 1 & 0 & 0 & 0 \\
0 & 0 & 0 & 0 & 0 & 0 & 0 & 0 & -1 & 1 & 0 & 0 & 0 & 0 & 0 & 0 & 0 & 0 & -1 & 0 & 0 & 1 & 0 & 0 \\
0 & 0 & 0 & 0 & 0 & 0 & 0 & 0 & 0 & -1 & 1 & 0 & 0 & 0 & 0 & 0 & 0 & 0 & 0 & -1 & 0 & 0 & 1 & 0 \\
0 & 0 & 0 & 0 & 0 & 0 & 0 & 0 & 0 & 0 & -1 & 1 & 0 & 0 & 0 & 0 & 0 & 0 & 0 & 0 & -1 & 0 & 0 & 1
\end{pmatrix}.$$

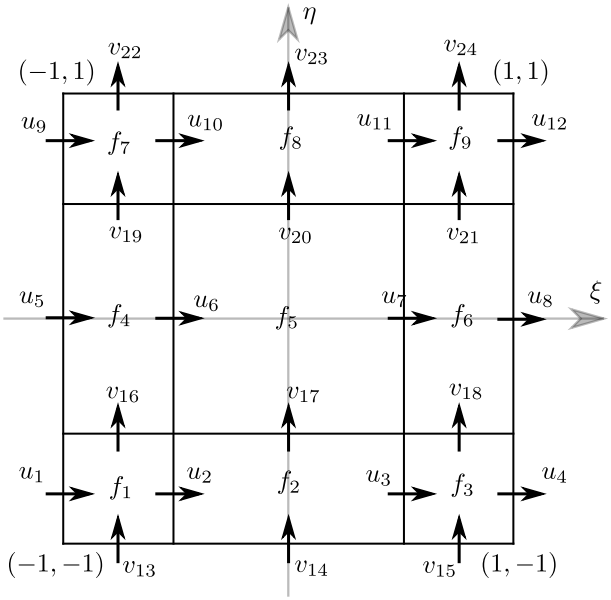

Figure 1: A reference domain partitioned by the Gauss-Lobatto-Legendre (GLL) nodes of order $N = 3$.

For more information on incidence matrices, we refer to [1, 8, 9, 10].

The trace variable $\mathrm{tr}_{\mathrm{div}}\boldsymbol{u}$ can be discretized as

$$\mathrm{tr}_{\mathrm{div}}\boldsymbol{u}_h = \left\{ \sum_{i=1}^{N} v_i^{\mathsf{s}} e_i(\xi), \sum_{i=1}^{N} v_i^{\mathsf{n}} e_i(\xi), \sum_{i=1}^{N} u_i^{\mathsf{w}} e_i(\eta), \sum_{i=1}^{N} u_i^{\mathsf{e}} e_i(\eta) \right\}, \tag{8}$$

where $v_i^{\mathsf{s}} = -\int_{\xi_{i-1}}^{\xi_i} v(\xi,-1)\mathrm{d}\xi$, $v_i^{\mathsf{n}} = \int_{\xi_{i-1}}^{\xi_i} v(\xi,1)\mathrm{d}\xi$, $u_i^{\mathsf{w}} = -\int_{\eta_{i-1}}^{\eta_i} u(-1,\eta)\mathrm{d}\eta$ and $u_i^{\mathsf{e}} = \int_{\eta_{i-1}}^{\eta_i} u(1,\eta)\mathrm{d}\eta$. It is easy to see that there is a linear operator, $\mathbb{N}$, such that

$$\underline{\boldsymbol{u}}_{\mathrm{tr}} = \mathbb{N}\underline{\boldsymbol{u}},$$

where $\underline{\boldsymbol{u}}_{\mathrm{tr}} = (\underline{v}_i^{\mathsf{s}}, \underline{v}_i^{\mathsf{n}}, \underline{u}_i^{\mathsf{w}}, \underline{u}_i^{\mathsf{e}})^T$ is the column vector of expansion coefficients in (8). For instance, the matrix $\mathbb{N}$ for the reference domain in Figure 1 is given by

$$\mathbb{N} = \begin{pmatrix}
0 & 0 & 0 & 0 & 0 & 0 & 0 & 0 & 0 & 0 & 0 & 0 & -1 & 0 & 0 & 0 & 0 & 0 & 0 & 0 & 0 & 0 & 0 & 0 \\
0 & 0 & 0 & 0 & 0 & 0 & 0 & 0 & 0 & 0 & 0 & 0 & 0 & -1 & 0 & 0 & 0 & 0 & 0 & 0 & 0 & 0 & 0 & 0 \\
0 & 0 & 0 & 0 & 0 & 0 & 0 & 0 & 0 & 0 & 0 & 0 & 0 & 0 & -1 & 0 & 0 & 0 & 0 & 0 & 0 & 0 & 0 & 0 \\
0 & 0 & 0 & 0 & 0 & 0 & 0 & 0 & 0 & 0 & 0 & 0 & 0 & 0 & 0 & 0 & 0 & 0 & 0 & 0 & 0 & 1 & 0 & 0 \\
0 & 0 & 0 & 0 & 0 & 0 & 0 & 0 & 0 & 0 & 0 & 0 & 0 & 0 & 0 & 0 & 0 & 0 & 0 & 0 & 0 & 0 & 1 & 0 \\
0 & 0 & 0 & 0 & 0 & 0 & 0 & 0 & 0 & 0 & 0 & 0 & 0 & 0 & 0 & 0 & 0 & 0 & 0 & 0 & 0 & 0 & 0 & 1 \\
-1 & 0 & 0 & 0 & 0 & 0 & 0 & 0 & 0 & 0 & 0 & 0 & 0 & 0 & 0 & 0 & 0 & 0 & 0 & 0 & 0 & 0 & 0 & 0 \\
0 & 0 & 0 & 0 & -1 & 0 & 0 & 0 & 0 & 0 & 0 & 0 & 0 & 0 & 0 & 0 & 0 & 0 & 0 & 0 & 0 & 0 & 0 & 0 \\
0 & 0 & 0 & 0 & 0 & 0 & 0 & 0 & -1 & 0 & 0 & 0 & 0 & 0 & 0 & 0 & 0 & 0 & 0 & 0 & 0 & 0 & 0 & 0 \\
0 & 0 & 0 & 1 & 0 & 0 & 0 & 0 & 0 & 0 & 0 & 0 & 0 & 0 & 0 & 0 & 0 & 0 & 0 & 0 & 0 & 0 & 0 & 0 \\
0 & 0 & 0 & 0 & 0 & 0 & 0 & 1 & 0 & 0 & 0 & 0 & 0 & 0 & 0 & 0 & 0 & 0 & 0 & 0 & 0 & 0 & 0 & 0 \\
0 & 0 & 0 & 0 & 0 & 0 & 0 & 0 & 0 & 0 & 0 & 1 & 0 & 0 & 0 & 0 & 0 & 0 & 0 & 0 & 0 & 0 & 0 & 0
\end{pmatrix}.$$

Like $\mathbb{E}^{21}$, $\mathbb{N}$ also only depends on the labeling of expansion coefficients and only contains entries of -1, 0 and 1.

4.2 Dual representations

Let scalar functions p_h and q_h be expanded in terms of $\{e_i(\xi)e_j(\eta)\}$. The L^2-inner product of them is given by

$$(p_h, q_h)_{L^2(\Omega_{\text{ref}})} = \int_{\Omega_{\text{ref}}} p_h(\xi,\eta) q_h(\xi,\eta) \mathrm{d}\xi \mathrm{d}\eta = \underline{p}^T \mathbb{M}^{(2)} \underline{q},$$

where $\mathbb{M}^{(2)}$ is the mass matrix. We define the dual basis functions as

$$\left[\widetilde{e_1(\xi)e_1(\eta)}, \cdots, \widetilde{e_N(\xi)e_N(\eta)}\right] := \left[e_1(\xi)e_1(\eta), \cdots, e_N(\xi)e_N(\eta)\right] \mathbb{M}^{(2)^{-1}},$$

It follows from the fact $\mathbb{M}^{(2)}$ is surjective (therefore, is also injective) that the finite dimensional space spanned by the dual basis functions $\left[\widetilde{e_1(\xi)e_1(\eta)}, \cdots, \widetilde{e_N(\xi)e_N(\eta)}\right]$ is isomorphic to the finite dimensional space spanned by $[e_1(\xi)e_1(\eta), \cdots, e_N(\xi)e_N(\eta)]$. Now, if we expand p_h in terms of the dual basis functions $\left\{\widetilde{e_i(\xi)e_j(\eta)}\right\}$, we have

$$(\tilde{p}_h, q_h)_{L^2(\Omega_{\text{ref}})} = \underline{\tilde{p}}^T \underline{q},$$

where $\underline{\tilde{p}} = \mathbb{M}^{(2)} \underline{p}$. Furthermore, if

$$q_h = \text{div } \boldsymbol{v}_h,$$

where $\boldsymbol{v}_h$ is expanded by the primal basis functions $\{h_i(\xi)e_j(\eta), e_i(\xi)h_j(\eta)\}$, we have

$$(\tilde{p}_h, \text{div } \boldsymbol{v}_h)_{L^2(\Omega_{\text{ref}})} = \underline{\tilde{p}}^T \mathbb{E}^{2,1} \underline{\boldsymbol{v}}.$$

For the trace variables which are expanded in terms of one-dimensional edge functions; see (8), we can compute the mass matrix $\mathtt{M}$ and define the dual basis functions as

$$\left[\widetilde{e_1(s)}, \cdots, \widetilde{e_N(s)}\right] := \left[e_1(s), \cdots, e_N(s)\right] \mathtt{M}^{-1}.$$

Note that we use $e_i(s)$ to represent either $e_i(\xi)$ or $e_i(\eta)$. Let discrete vector $\boldsymbol{q}_h$ be expanded by primal basis functions $\{h_i(\xi)e_j(\eta), e_i(\xi)h_j(\eta)\}$ and discrete trace variable $\tilde{\phi}_h$ be expanded by $\left\{\widetilde{e_i(s)}\right\}$. We have

$$\left(\tilde{\phi}_h, \text{tr}_{\text{div}} \boldsymbol{q}_h\right)_{L^2(\partial\Omega_{\text{ref}})} = \underline{\tilde{\phi}}^T \mathbb{N} \underline{\boldsymbol{q}} = \underline{\tilde{\phi}}^T \underline{\boldsymbol{q}}_{\text{tr}}.$$

For more details about dual polynomials, we refer to [7].

5 THE DISCRETE HYBRID MIXED FORMULATION

In this section, we use the basis functions derived in the last section to discretize the hybrid mixed formulation (3). Given the domain Ω, we first set up a proper conforming (curvilinear) quadrilateral mesh Ω_h. The finite dimensional space spanned by basis functions $\{h_i(\xi)e_j(\eta), e_i(\xi)h_j(\eta)\}$ is chosen to approximate $H(\text{div}, \Omega_h)$, the finite dimensional

space spanned by dual basis functions $\left\{\widetilde{e_i(\xi)e_j(\eta)}\right\}$ is chosen to approximate $H^1(\Omega_h)$, and finite space spanned by dual basis functions $\left\{\widetilde{e_i(s)}\right\}$ is chosen to approximate $H^{1/2}(\partial\Omega_h)$. Remember that all basis functions presented in the last section are for the reference domain. In different elements, the basis functions change due to the mapping from the reference domain to them. How to derive the basis functions in arbitrary elements is explained in [5, §4]. The basis functions mentioned here refer to the basis functions in each element of the mesh Ω_h.

With above discretizations, the discrete hybrid mixed formulation is written as

$$\begin{pmatrix} \mathbb{M}^{(1)} & \mathbb{E}^{2,1^T} & -\mathbb{N}_I^T \\ \mathbb{E}^{2,1} & 0 & 0 \\ -\mathbb{N}_I & 0 & 0 \end{pmatrix} \begin{pmatrix} \underline{\boldsymbol{u}} \\ \underline{\varphi} \\ \underline{\check{\varphi}} \end{pmatrix} = \begin{pmatrix} \mathbb{N}_B^T \underline{\hat{\varphi}} \\ -\underline{f} \\ 0 \end{pmatrix}, \tag{9}$$

where $\mathbb{M}^{(1)}$ is the mass matrix with respect to the basis functions $\{h_i(\xi)e_j(\eta), e_i(\xi)h_j(\eta)\}$ and the matrix $\mathbb{N}$ has been divided into two parts, $\mathbb{N}_I$ and $\mathbb{N}_B$, corresponding to the internal interface $\partial\Omega_h \backslash \partial\Omega$ and the domain boundary $\partial\Omega$. Note that $\mathbb{M}^{(1)}$, $\mathbb{E}^{2,1}$ and $\mathbb{N}$ here are all assembled matrices. It is worth to repeat that, assuming the same order basis functions is used for all elements, only for $\mathbb{M}^{(1)}$, the contribution of each element depends on the size, shape and metric of the element. Contributions of all elements for $\mathbb{E}^{2,1}$ are the same as well as for $\mathbb{N} = \mathbb{N}_I + \mathbb{N}_B$. In addition, with proper labeling of degrees of freedom, we can obtain element-wise-block-diagonal $\mathbb{M}^{(1)}$ and $\mathbb{E}^{2,1}$, which means the matrix computation for them is easily parallelizable. Furthermore, $\mathbb{E}^{2,1}$ and $\mathbb{N}$ are extremely sparse and only contain non-zero entries of -1, $+1$, which usually is a feature of low order finite difference (volume) methods.

We can easily eliminate $\underline{\boldsymbol{u}}$ and $\underline{\varphi}$ from (9) and obtain a system for the discrete interface variable $\underline{\check{\varphi}}$, [3],

$$\mathbb{H}\underline{\check{\varphi}} = \mathbb{F}, \tag{10}$$

where

$$\begin{aligned}
\mathbb{H} &= -\mathbb{N}_I \mathbb{M}^{(1)^{-1}} \left[\mathbb{M}^{(1)} - \mathbb{E}^{2,1^T} \left(\mathbb{E}^{2,1} \mathbb{M}^{(1)^{-1}} \mathbb{E}^{2,1^T} \right)^{-1} \mathbb{E}^{2,1} \right] \mathbb{M}^{(1)^{-1}} \mathbb{N}_I^T, \\
\mathbb{F} &= \mathbb{F}_{\hat{\varphi}} + \mathbb{F}_f, \\
\mathbb{F}_{\hat{\varphi}} &= \mathbb{N}_I \mathbb{M}^{(1)^{-1}} \left[\mathbb{M}^{(1)} - \mathbb{E}^{2,1^T} \left(\mathbb{E}^{2,1} \mathbb{M}^{(1)^{-1}} \mathbb{E}^{2,1^T} \right)^{-1} \mathbb{E}^{2,1} \right] \mathbb{M}^{(1)^{-1}} \mathbb{N}_B^T \underline{\hat{\varphi}}, \\
\mathbb{F}_f &= -\mathbb{N}_I \mathbb{M}^{(1)^{-1}} \mathbb{E}^{2,1^T} \left(\mathbb{E}^{2,1} \mathbb{M}^{(1)^{-1}} \mathbb{E}^{2,1^T} \right)^{-1} \underline{f}.
\end{aligned}$$

Because that both $\mathbb{M}^{(1)}$ and $\mathbb{E}^{2,1}$ are element-wise-block-diagonal, inverting $\mathbb{M}^{(1)}$ and $\mathbb{E}^{2,1}\mathbb{M}^{(1)^{-1}}\mathbb{E}^{2,1^T}$ can be done efficiently by inverting local matrices in parallel. After $\underline{\check{\varphi}}$ is solved, the remaining local problems for $\underline{\boldsymbol{u}}$ and $\underline{\varphi}$ are trivial as the inverse of their Schur complements, $(\mathbb{E}^{2,1}\mathbb{M}^{(1)^{-1}}\mathbb{E}^{2,1^T})^{-1}$, is already computed.

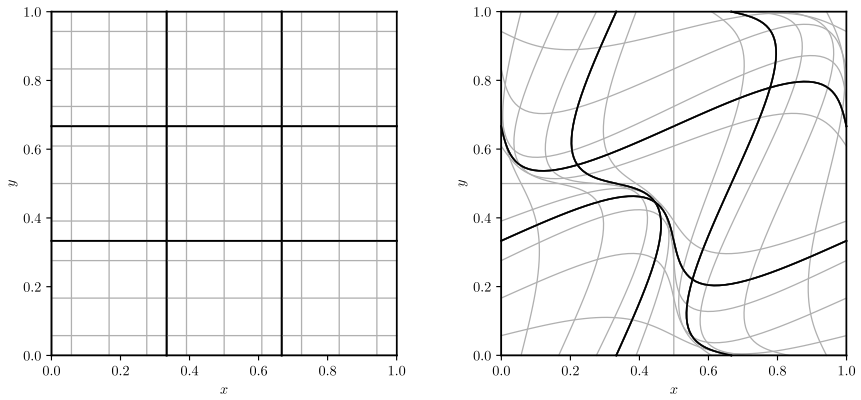

Figure 2: Meshes for $N = 4$, $K = 3^2$. Left: $c = 0$. Right: $c = 0.3$. The black lines represent element boundaries and the gray lines represent the GLL mesh.

6 NUMERICAL EXPERIMENTS

In this section, we will present two numerical experiments. The first one is a manufactured numerical test case to investigate the *hp*-convergence of the method on both orthogonal and distorted meshes. The second test case is a potential flow through a domain with boundaries interpolated by cubic splines.

6.1 Manufactured numerical test case

Consider a domain $\Omega = [0, 1]^2$ and an exact solution

$$\varphi_{\text{exact}} = \cos(3\pi x e^y).$$

We solve the Poisson problem in Ω with $f_{\text{exact}} = -\text{div grad } \varphi_{\text{exact}}$ prescribed all over the domain and $\hat{\varphi} = \text{tr}_{\text{grad}}\varphi_{\text{exact}}$ imposed along the boundary. To obtain meshes in Ω, we first divide the reference domain $\Omega_{\text{ref}} = [-1, 1]^2$ into K elements uniformly. Within all elements, the GLL mesh of the same order N is generated; see Figure 1. Then we transform Ω_{ref} into Ω with mapping

$$\begin{cases} x = \dfrac{1}{2} + \dfrac{1}{2}\left[\xi + c\sin(\pi\xi)\sin(\pi\eta)\right] \\ y = \dfrac{1}{2} + \dfrac{1}{2}\left[\eta + c\sin(\pi\xi)\sin(\pi\eta)\right] \end{cases},$$

where c is the deformation coefficient. When $c = 0$, the mesh is orthogonal. When $c > 0$, the mesh becomes curvilinear. Two examples are shown in Figure 2.

H^1-error of solution φ_h, $H(\text{div})$-error of solution $\boldsymbol{u}_h$ and L^2-error of $(\text{div}\boldsymbol{u}_h + f_h)$ under *hp*-refinements are presented in Figure 3. From this figure, we can see that, in both orthogonal and distorted meshes, exponential convergence under p-refinements and optimal convergence rates under h-refinements are obtained for both $\|\varphi_h\|_{H^1-\text{error}}$ and $\|\boldsymbol{u}_h\|_{H(\text{div})-\text{error}}$. The computing of $\|\varphi_h\|_{H^1-\text{error}}$ uses the solution of φ_h and its trace values $\check{\varphi}_h$ and $\hat{\varphi}_h$. Recall the physical meaning of $\check{\varphi}$ in (3). For more details, see [7]. In addition, the divergence relation $\text{div}\,\boldsymbol{u}_h + f_h = 0$ is always conserved to the machine precision, which proves the discrete div operator, incidence matrix $\mathbb{E}^{2,1}$, is exact.

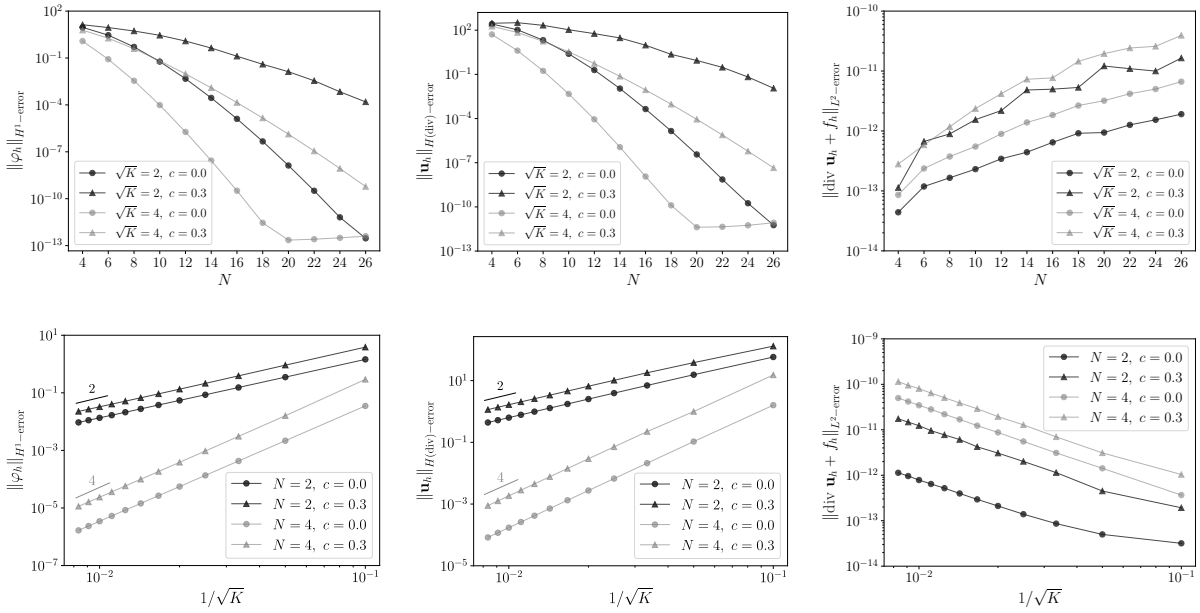

Figure 3: $\|\varphi_h\|_{H^1-\text{error}}$, $\|\boldsymbol{u}_h\|_{H(\text{div})-\text{error}}$ and $\|\text{div}\ \boldsymbol{u}_h + f_h\|_{L^2-\text{error}}$ under p-refinements (top) and h-refinements (bottom).

6.2 Potential flow in a domain with spline interpolation boundaries

Our second numerical experiment is to solve a potential flow through a domain, whose lower, upper and inner boundaries are interpolated with cubic splines. Sequences of samples for the interpolation are shown in Table 1. The left boundary (inlet) is given by line segment $\{x = 0, 0 \leq y \leq 1.5\}$, and the right boundary (outlet) is given by line segment $\{x = 3, 0 \leq y \leq 1.5\}$; see Figure 4. To make this problem well-posed, we define the upper, lower and inner boundaries to be free-slip walls, $\boldsymbol{u} \cdot \boldsymbol{n} = 0$, and define the potential $\hat{\varphi} = 0$ at left boundary and $\hat{\varphi} = 10$ at the right boundary. The source term, f, is set to be zero.

The domain is divided into K elements, and mappings which map the reference domain into elements are obtained using the transfinite interpolation [6]. Within each element, a GLL mesh of order N is used. An example of the mesh for $K = 16$ is shown in Figure 4(a), and the h-refinement is done by uniformly dividing each element of this mesh into multiple elements at the level of reference domain (as we did in last test case).

The problem is solved in ph-refined meshes. An example of the velocity solution vector field is presented in Figure 4(b). Because of the exact discretization of the divergence operator with the incidence matrix $\mathbb{E}^{2,1}$, $\text{div}\ \boldsymbol{u}_h = -f_h = 0$ is pointwise-conserved all over the domain. As a result, the flux going into the domain through the left boundary is always equal to the flux leaving the domain through the right boundary. Results of fluxes through the domain are given in Table 2 which shows the flux converges to 3.03141.

Table 1: Coordinates of samples.

Boundary	Sequence of samples.
Lower	$(0,0)$, $(0.11,0.01)$, $(0.20,0.12)$, $(0.61,-0.05)$, $(0.69,0.16)$, $(0.82,0)$, $(0.91,0.15)$, $(1.01,-0.05)$, $(1.21,-0.15)$, $(1.30,0.13)$, $(1.48,0.22)$, $(1.65,-0.05)$, $(1.85,0.02)$, $(2,0.15)$, $(2.11,-0.03)$, $(2.36,0.31)$, $(2.50,0.13)$, $(2.71,0.12)$, $(2.91,0)$, $(3,0)$.
Upper	$(0,1.5)$, $(0.09,1.51)$, $(0.17,1.32)$, $(0.43,1.45)$, $(0.58,1.36)$, $(0.83,1.50)$, $(0.93,1.75)$, $(1.14,1.52)$, $(1.18,1.45)$, $(1.33,1.33)$, $(1.4,1.64)$, $(1.59,1.45)$, $(1.88,1.37)$, $(1.92,1.47)$, $(2.15,1.63)$, $(2.40,1.71)$, $(2.51,1.43)$, $(2.72,1.42)$, $(2.89,1.5)$, $(3,1.5)$.
Inner	$(1,0.5)$, $(1.11,0.35)$, $(1.32,0.55)$, $(1.62,0.66)$, $(1.85,0.45)$,$(1.98,0.5)$, $(2.1,0.55)$, $(1.95,0.75)$, $(1.9,0.99)$, $(1.79,1.05)$,$(1.6,0.88)$, $(1.33,1.09)$, $(0.95,1)$, $(0.93,0.95)$, $(1.09,0.76)$,$(0.89,0.65)$, $(1,0.5)$.

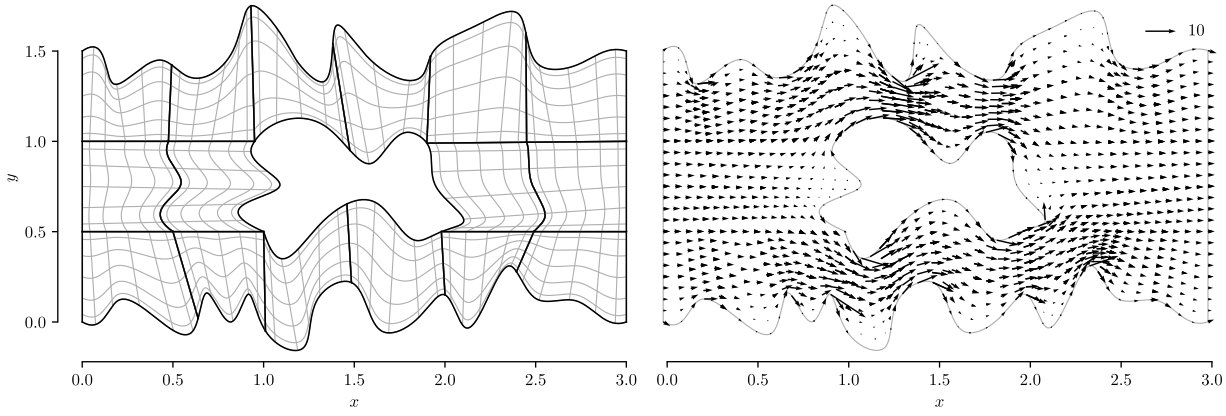

(a) (b)

Figure 4: (a): The domain and the mesh for $K = 16$, $N = 6$. (b): The vector field of the velocity solution for $K = 64$, $N = 16$.

Table 2: Fluxes through the domain.

N	Number of elements				
	16	64	256	576	1024
2	2.49949	2.92468	2.95905	3.01901	3.02207
4	2.95266	3.03115	3.02979	3.03123	3.03129
6	3.04810	3.02942	3.03120	3.03139	3.03139
8	3.01246	3.03047	3.03137	3.03140	3.03141
10	3.02062	3.03108	3.03141	3.03141	3.03141
12	3.03175	3.03137	3.03141	3.03141	3.03141
14	3.03045	3.03142	3.03141	3.03141	3.03141

REFERENCES

[1] Bochev, P. A discourse on variational and geometric aspects of stability of discretizations. *33rd Computational Fluid Dynamics Lecture Series*, (2003) VKI LS, 5.

[2] Carstensen, C., Demkowicz, L. and Gopalakrishnan, J. Breaking spaces and forms for the DPG method and applications including Maxwell equations. *Computers and Mathematics with Applications*, (2016) **72**(3): 494-522.

[3] Cockburn, B., and Gopalakrishnan, J. A characterization of hybridized mixed methods for second order elliptic problems. *SIAM Journal on Numerical Analysis*, (2004) **42**(1): 283-301.

[4] Gerritsma, M. Edge functions for spectral element methods. *Spectral and High Order Methods for Partial Differential Equations*. Springer, Berlin, Heidelberg, (2011) 199-207.

[5] Gerritsma, M., Palha, A., Jain, V. and Zhang, Y. Mimetic Spectral Element Method for Anisotropic Diffusion. *arXiv preprint*, (2018) arXiv:1802.04597.

[6] Gordon, W.J., and Charles A.H. Transfinite element methods: blending-function interpolation over arbitrary curved element domains. *Numerische Mathematik*, (1973) **21**(2): 109-129.

[7] Jain, V., Zhang, Y., Palha, A. and Gerritsma, M. Construction and application of algebraic dual polynomial representations for finite element methods. *arXiv preprint*, (2017) arXiv:1712.09472.

[8] Kreeft, J. and Gerritsma, M. Mixed mimetic spectral element method for Stokes flow: A pointwise divergence-free solution. *Journal of Computational Physics*, (2013) **240**: 284-309.

[9] Kreeft, J., Palha, A. and Gerritsma, M. Mimetic framework on curvilinear quadrilaterals of arbitrary order. *arXiv preprint*, (2011) arXiv:1111.4304.

[10] Palha, A., Rebelo, P.P., Hiemstra, R., Kreeft, J. and Gerritsma, M. Physics-compatible discretization techniques on single and dual grids, with application to the Poisson equation of volume forms. *Journal of Computational Physics*, (2014) **257**: 1394-1422.

[11] Pian, T.H. Derivation of element stiffness matrices by assumed stress distributions. *AIAA journal*, (1964) **2**(7), 1333-1336.

[12] Raviart, P.A. and Thomas, J.M. Primal hybrid finite element methods for 2nd order elliptic equations. *Mathematics of computation*, (1977) **31**(138), 391-413.

[13] Tinsley, O.J. and Demkowicz, L. *Applied functional analysis*, Chapman and Hall/CRC, 2017.